Original Article

Evaluation of bone marrow infiltration in multiple myeloma using whole-body diffusion-weighted imaging and T1-weighted water-fat separation Dixon

Xiaodong Ji[1,2#], Wenyang Huang[3#], Huazheng Dong[4], Zhiwei Shen[5], Meizhu Zheng[6], Dehui Zou[3], Wen Shen[2*], Shuang Xia[2*]

[1]Radiology Department, First Central Clinical College, Tianjin Medical University, Tianjin, China; [2]Department of Radiology, Tianjin First Central Hospital, School of Medicine, Nankai University, Tianjin, China; [3]State Key Laboratory of Experimental Hematology, Institute of Hematology & Blood Diseases Hospital, Chinese Academy of Medical Sciences & Peking Union Medical College (CAMS & PUMC), Tianjin, China; [4]Radiology Department, Tianjin Academy of Traditional Chinese Medicine Affiliated Hospital, Tianjin, China; [5]Philips Healthcare, World Profit Centre, Beijing, China; [6]Radiological Department, Third Central Hospital of Tianjin, Tianjin, China

[#]These authors contributed equally to this work as co-first authors.

[*]These authors contributed equally to this work as co-corresponding authors.

Correspondence to: Shuang Xia; Wen Shen. Department of Radiology, Tianjin First Central Hospital, School of Medicine, Nankai University, 24 Fukang Road, Nankai District, Tianjin 300192, China. Email: xiashuang77@163.com; shenwen66happy@163.com.

Background: Multiple myeloma (MM) is a blood cancer caused by the unlimited proliferation of intramedullary plasma cells. The presence of focal lesions (FLs) is presumed to be a more relevant factor for patient outcomes and risk distribution than diffuse bone marrow signal abnormalities. Signal changes in these FLs also have a good correlation with prognosis. As the cell density increased, a lower apparent diffusion coefficient (ADC) value was found with the diffusion-weighted imaging (DWI) sequence. Therefore, whole-body magnetic resonance imaging (MRI) with DWI sequences is sensitive to cell density and viability and may be vital for disease detection and therapy response assessments. However, the correlation between the DWI signal and the degree of bone destruction and the proportion of bone marrow plasma cells (BMPC) was still unclear in patients with MM. Water-fat separation MRI is used mainly for evaluating liver and bone marrow fat quantification, and fat quantification in other diseases. Meanwhile, it is also possible to assess the extent of bone marrow invasion in medullary lesions. This study aimed to investigate the correlation between ADC values from whole-body DWI and water/fat MRI signals from T1-weighted water-fat separation in evaluating bone marrow infiltration in patients with MM.

Methods: The study included 35 patients with MM who underwent whole-body DWI and T1-weighted water-fat separation Dixon examinations before therapy. The ADC values, normalized fat signal intensity (nMfat), normalized water molecular signal intensity (nMwater), and normalized fat fraction (nFF) of the thoracolumbar spine was measured in FLs and the normal-appearing bone marrow (NABM). The differences in values were compared using the independent-samples *t*-test. The correlation between ADC values and water-fat MRI signals was estimated using the Pearson or Spearman correlation test. The correlation between the MRI above parameters and proportions of BMPC was also explored.

Results: Statistically significant differences were found between the mean ADC values in FLs and NABM (0.72 *vs.* 0.33 mm^2/s, P<0.0001). Significantly elevated nMwater values and decreased nMfat and nFF values were observed in FLs; no correlations were found in NABM (P>0.05). The ADC value highly correlated with nMfat and nFF values and moderately with the nMwater value in FLs (r=–0.899, –0.834, 0.642, respectively, P<0.0001). Correlations were also observed between the proportion of BMPC and MRI parameters in MM (r=0.984, 0.716, –0.938, and –0.905, respectively, P<0.05).

Conclusions: The ADC value combined with water-fat separation parameters could be used for evaluating thoracolumbar bone marrow infiltration in MM. All parameters correlated with the proportion of BMPC, which helped assess the early response in MM therapy.

Keywords: Apparent diffusion coefficient (ADC); whole-body diffusion-weighted imaging (whole-body DWI); multiple myeloma (MM); normalized fat fraction (nFF); water-fat separation Dixon technique

Submitted Feb 16, 2020. Accepted for publication Oct 16, 2020.
doi: 10.21037/qims-20-289
View this article at: http://dx.doi.org/10.21037/qims-20-289

Introduction

Multiple myeloma (MM) is a type of blood cancer caused by intramedullary plasma cells' unrestrained proliferation. Many malignant plasma cells in the bone marrow can cause osteoporosis, osteolytic destruction, and pathological fractures. Therapy is necessary for patients with nodular lesions of diameter >5 mm (1,2). The presence of focal lesions (FLs) is presumed to be a more relevant factor for patient outcomes and risk distribution than diffuse bone marrow signal abnormalities (1). Signal changes in these FLs also have a good correlation with prognosis (3,4).

The ^{18}F-fluorodeoxyglucose with positron emission tomography/computed tomography (^{18}F-FDG PET/CT) is a preferred functional imaging method for evaluating and detecting the therapeutic effects on MM due to its good performance in distinguishing between metabolically active cells and inactive cells (5). Besides evaluating bone marrow lesions in patients with MM, ^{18}F-FDG PET/CT has also been widely applied to other clinical scenarios, such as bone disease detection (6), initial staging and therapy assessment (7), evaluation of the prognosis of myeloma (8), and determination of the remission status (9). However, FDG PET-CT has some limitations, including it being false negative in detecting diffuse bone marrow infiltration and false positive in detecting inflammatory lesions (10), and has insufficient lesion detection ability compared with magnetic resonance imaging (MRI) (11). Also, the PET/CT involves a further dose of radiation (12).

As the cell density increased, a lower apparent diffusion coefficient (ADC) value was found with the diffusion-weighted imaging (DWI) sequence. Therefore, whole-body MRI with DWI sequences is sensitive to cell density and viability and may be vital for disease detection and therapy response assessments (13). The DWI is also recommended for assessing the depth of bone marrow infiltration (14), identifying different myeloma types (15), and performing the risk stratification of asymptomatic myeloma (3). However, the correlation between the DWI signal and the degree of bone destruction and the proportion of bone marrow plasma cells (BMPC) was still unclear in patients with MM.

Chemical shift-encoding-based water-fat MRI offered the invaluable advantage of providing spatially resolved bone marrow fat quantification (16). Water-fat separation MRI is used mainly for evaluating liver fat quantification (17), bone marrow fat quantification (18), and fat quantification in other diseases (19,20); it is also possible to assess the extent of bone marrow invasion in medullary lesions (21). Several studies have evaluated the relationship among ADC value, FF, and D_{slow} in MRI, as well as the standardized uptake value (SUV) value in PET, in normal bone marrow (22) and bone marrow lesions in tumor patients (23), while distinguishing benign and malignant bone marrow lesions (24).

Few studies investigated the correlation between ADC and T1-weighted water-fat separation MRI for MM and explored whether this difference was consistent with different proportions of BMPC. It was hypothesized that a correlation existed between ADC values and the parameters of water-lipid separation in the thoracic and lumbar vertebrae. Moreover, it was also assumed that a correlation existed between MRI parameters and the proportion of BMPC in MM. This study aimed to explore the possible correlation between ADC values and water/fat MRI signals in FLs of the thoracolumbar spine in MM. The study also investigated the correlation between MRI parameters and the proportion of BMPC in MM, thus helping assess the proliferation of bone marrow plasmacytoma using MRI.

Methods

Patient population

The ethics committee approved this study of the

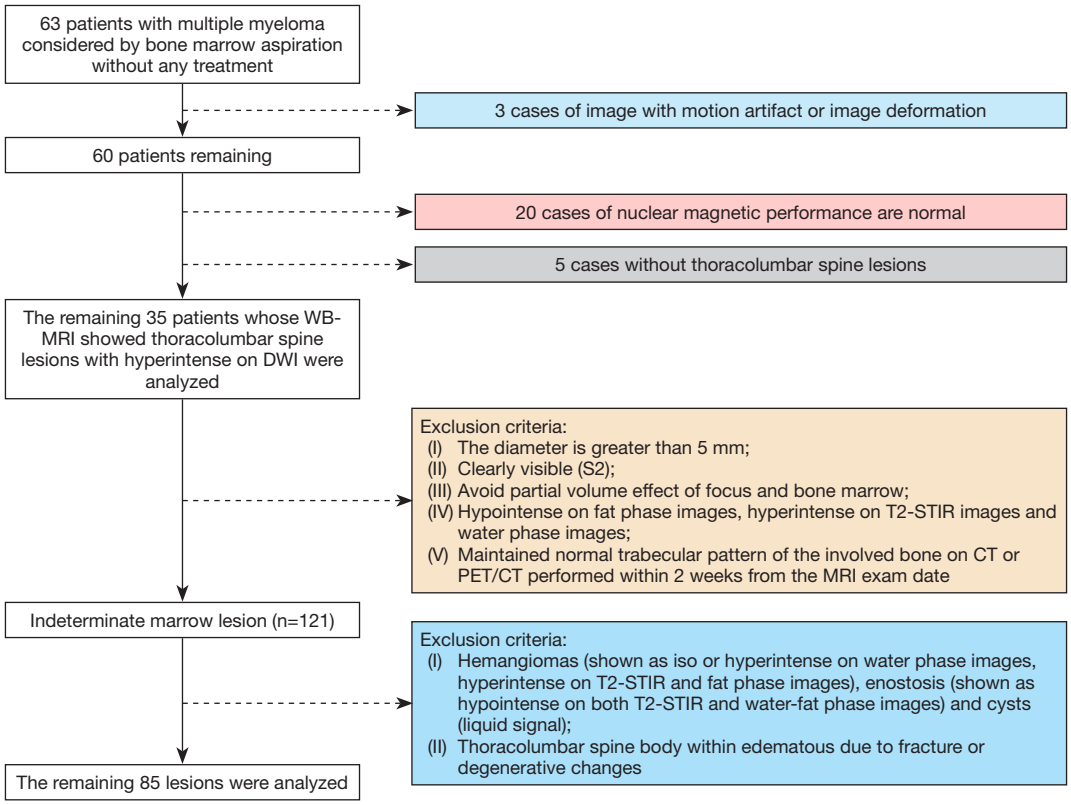

Figure 1 Flow chart of participants and FL selection. WB, whole body; MRI, magnetic resonance imaging; DWI, diffusion-weighted imaging; STIR, short-time inversion recovery; PET, positron emission tomography; CT, computed tomography; FL, focal lesion.

First Central Hospital of Tianjin (2017N078KY); all participants provided written informed consent form before examination. All patients underwent whole-body DWI and water-fat separation Dixon examination before treatment. Marrow biopsy was also taken within 1 week before or after MRI. A retrospective review was performed by 2 radiologists (S Xia, X Ji, with 22 and 10 years of experience, respectively) to determine focal indeterminate marrow abnormalities in consensus.

The inclusion criteria for focal indeterminate marrow abnormalities in the present study were as follows: (I) focal marrow abnormalities on conventional MRI; (II) normal trabecular pattern of the involved bone maintained on CT or PET/CT performed within 2 weeks from the MRI examination date; (III) no specific feature for malignant lesions: no cortical violation or extra-osseous soft-tissue extension on MRI; and (IV) no specific imaging features for benign lesions, such as hemangioma, bone island, Modic type 1 vertebral endplate change or Schmorl's node in the spines, cystic lesion, osteonecrosis, and obvious benign tumors with specific imaging findings in the long bone.

From February 2015 to July 2017, all 63 patients with MM confirmed by pathology were included in the study. Among these 63 MM patients, 20 were excluded due to normal MRI findings, 3 were excluded due to images with motion artifacts or deformation, and another 5 were excluded because they had no thoracolumbar lesions. Finally, the study included 35 patients with multinodular lesions in the thoracolumbar spine on whole-body DWI; the selection of patients and lesions are shown in *Figure 1*.

MRI parameters

All data were analyzed on a 3.0 T magnetic resonance scanner (Ingenia, Philips Healthcare, Best, The Netherlands) with a 20-channel head and neck coil as well as a 32-channel phased-array coil. A respiratory gating scheme was constructed to ensure a high signal-to-noise ratio (SNR). The MRI protocol for bone marrow assessment included pulse sequences such as the whole-body DWI, short-time

Table 1 MRI parameters, exemplarily of sections with the longest acquisition time

Parameters	FOV (mm)	Matrix size	Thickness (mm)	TR/TE/TI (ms)	Flip angle	Slice (mm)	Scan time per segment (m)
DWI	340×398	96×111	6	6,483/65/220	180	77	2.5
STIR	340×398	212×220	6	6,698/70/230	180	33	1
T1-Dixon	340×398	196×224	6	3.4/1.14 (TE1)/2.0 (TE2)	10	33	3

MRI, magnetic resonance imaging; FOV, field of view; TR, repetition time; TE, echo time; TI, inversion time; DWI, diffusion-weighted imaging; STIR, short-time inversion recovery.

inversion recovery (STIR), and whole-body T1-weighted Dixon technique. The MRI parameters of the DWI imaging, STIR imaging and T1-weighted modified Dixon (mDixon) imaging are summarized in *Table 1*. Coronal images were acquired with a DWI scan time of 15 min, a STIR scan time of 6 min and a T1-weighted Dixon scan time of 18 min. Once thoracolumbar lesions were found, the sagittal T2-weighted imaging Dixon protocol was also performed.

MRI processing and analysis

Regarding the criteria to select lesions, the focal pattern was characterized by 2 or more focal alterations in bone marrow on the whole-body DWI images (1) with a lower signal intensity than the normal bone marrow. The lesions in MM were also diagnosed as hypointense on T1 images and hyperintense on T2-STIR images.

The slice with the lesion's largest area was chosen to draw the region of interest (ROI) manually. The ROI of the lesion was drawn as the center of the image with a diameter of >5 mm in the thoracolumbar spine. Then, the ROI of the lesion was replicated and placed in the adjacent NABM around the lesion. Finally, ROIs of the FLs and NABM were also copied to the ADC maps and the fat and water images. In the fat and water images, the ROI was also copied to the fat tissue with the lesion's same phase direction. Each ROI was drawn and measured by the two radiologists 3 times with an interval of 1 month to avoid selection bias. The averaged value was used for calculation (result shown in the Supplementary material) (Figures S1-S7, Table S1). The ADC, fat signal intensity (Mfat), and water molecular signal intensity (Mwater) were measured on the MRI console. The fat fraction (FF) was calculated using the formula MFat/(MFat + Mwater), as proposed by Messiou *et al.* (25) and Latifoltojar *et al.* (26). The water/fat signal from the fat tissue in different participants had a good consistency and was treated as an internal reference to acquire the normalized MFat (nMfat), normalized Mwater (nMwater), and normalized fat fraction (nFF) signals of FLs and NABM in the thoracolumbar spine (*Figure 2A,B,C,D*).

Bone marrow examination

The BMPC were collected from bone marrow biopsy specimens of the bilateral posterior superior iliac spine.

Statistical analysis

Statistical analysis was performed using SPSS version 22.0 (SPSS Inc., IBM, Chicago, IL, USA) and GraphPad Prism version 7 (GraphPad Software, La Jolla, CA, USA). A normal distribution test was performed using the Kolmogorov-Smirnov test method. The differences in parameters between FLs and NABM were tested using the *t*-test or Mann-Whitney U test depending on normal distribution. Mean, standard deviation, and median (range) were measured to describe parameters. The correlation between the two groups was evaluated using the Pearson or Spearman correlation test. When the P value was <0.05, the difference was deemed statistically significant.

Results

Patient demographics

A total of 35 patients with multinodular lesions in the thoracolumbar spine were enrolled. These included 16 patients whose hemoglobin index was <10 g/dL and 8 patients whose creatinine level was >2 mg/dL. The demographic and clinical characteristics are shown in *Table 2*.

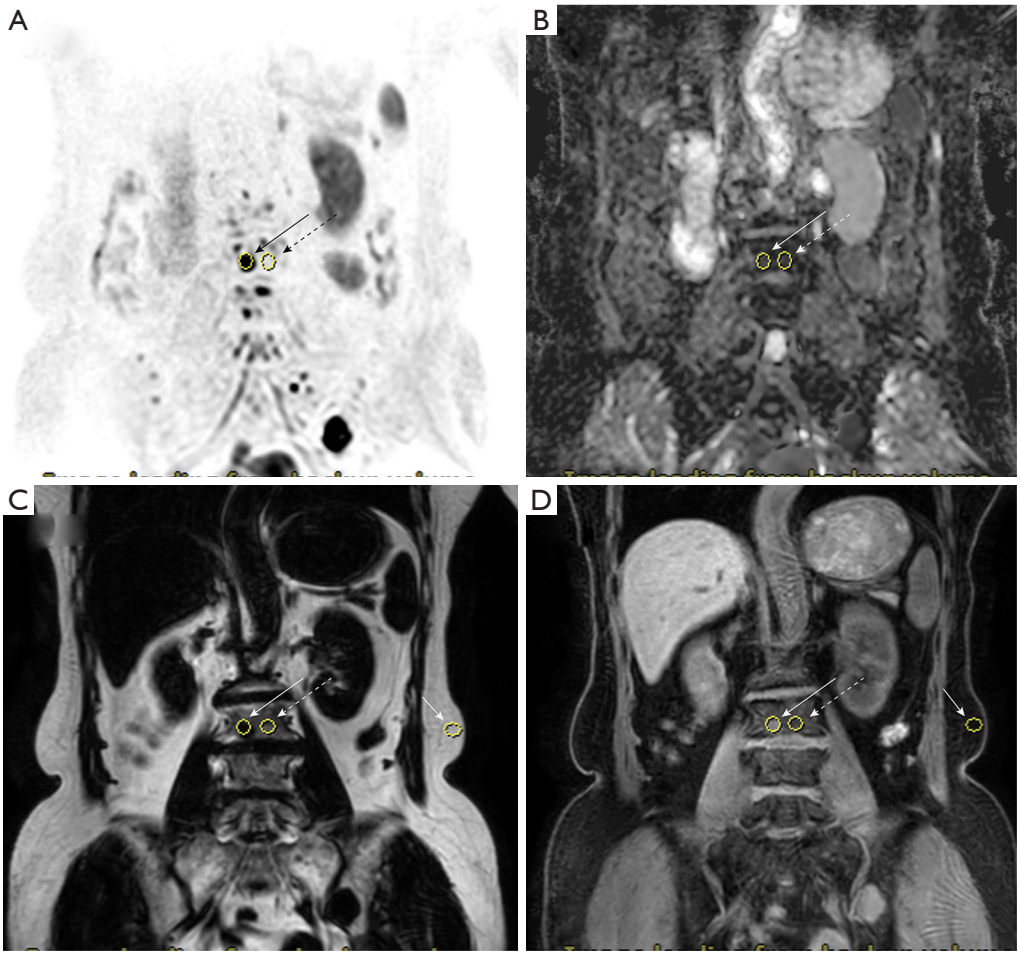

Figure 2 Images in a 65-year-old woman with multiple myeloma. (A) Coronal DWI image of the thoracolumbar spine with ROI of the FLs (the solid arrow) and NABM (the virtual arrow). The fat in the same phase direction with lesion was chosen as an internal reference to normalize the signal of Dixon. The ROI position of fat was also shown; coronal ADC image (B), fat phase (C), and water phase image (D) of the thoracolumbar spine. ROIs of the FLs and NABM located in the same position with those in DWI image. DWI, diffusion-weighted imaging; ROI, region of interest; FLs, focal lesions; NABM, normal appearing bone marrow; ADC, apparent diffusion coefficient.

Relationship between parameters of water-fat separation and ADC values

A total of 85 FLs were found. Of these, 30 lesions were detected in the thoracic spine, and 55 lesions were detected in the lumbar spine. Non-normal distribution of the parameters was found between FLs and NABM. The ADC value was 0.72 and 0.33 mm^2/s in FLs and NABM, respectively. A significant group difference was found (P<0.05); the nMwater value was 2.30 and 4.38 for FLs and NABM, respectively. A significant difference was also observed between the two groups (P<0.0001). Meanwhile, there was a statistical difference between nMfat and nFF between the two groups (P<0.0001). The nMfat and nFF values of the thoracolumbar spine were significantly higher in NABM than in FLs (P<0.0001) (*Figure 3A*,*B*,*C*,*D*). The results are shown in *Table 3*.

Relationship between ADC and nMfat, nMwater, and nFF values

A strong correlation was found between the ADC value and fat signal (nMfat and nFF) values (r=–0.899, –0.834, P<0.0001), while a moderate correlation was found between

Table 2 Demographics and clinical information of participants

Characteristic	Data
No. of patients	35
Sex	
Male	20
Female	15
Mean age (years) [range]	
Male	54.4 [36–67]
Female	49.9 [32–69]
Ig subtype	
IgG	22
IgA	8
IgD	5
ISS stage	
I	20
II	8
III	7
R-ISS stage	
I	18
II	11
III	6
HGB (<100 g/L)	16
Cr (>2 μmol/L)	3

R-ISS, Revised International Staging System; HGB, hemoglobin; Cr, creatinine.

Table 3 Comparison of parameters between FLs and NABM in patients with MM

Parameters of MRI	NABM	FLs	P
No. of lesions	85	85	–
ADC (mm^2/s)	0.33 (0.24–0.42)	0.72 (0.61–0.85)	<0.0001
nMfat	0.40 (0.36–0.44)	0.05 (0.04–0.07)	<0.0001
nMwater	2.30 (2.14–2.59)	4.38 (3.66–5.01)	<0.0001
nFF	0.15 (0.13–0.17)	0.01 (0.01–0.02)	<0.0001

NABM, normal-appearing bone marrow; FLs, focal lesions; ADC, apparent diffusion coefficient; nMfat, normalized fat signal intensity; nMwater, normalized water molecular signal intensity; nFF, normalized fat fraction.

the ADC and nMwater values in FLs (r=0.642, P<0.0001). However, no correlation was found between ADC value and water/fat signal (nMfat, nMwater, and nFF) values (r=–0.135, 0.115, and –0.145, all P>0.05) in NABM. The results are shown in *Table 4*.

The difference in parameters between two groups with different proportions of BMPC

The ADC, nMwater, nMfat, and nFF values in FLs and NABM were 0.83 *vs.* 0.59 mm^2/s, 0.48±0.01 *vs.* 0.40±0.01, 0.48±0.04 *vs.* 1.29±0.17, and 0.23 *vs.* 0.09, respectively. Statistically significant differences were found in ADC, nMwater, nMfat, and nFF values between the two groups with different proportions of BMPC. The results are shown

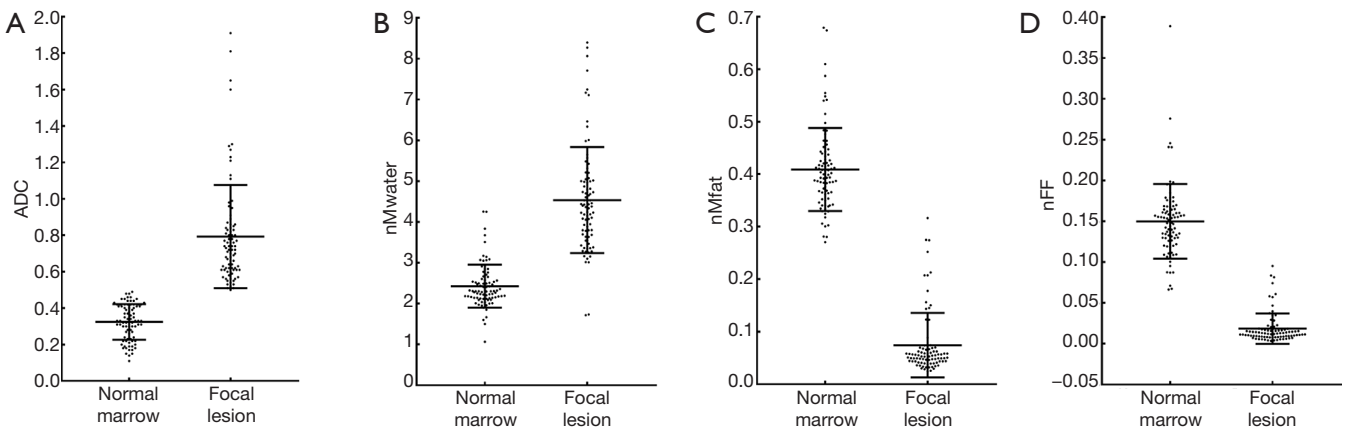

Figure 3 Scatter plot showed significant differences of ADC (A), nMwater (B), nMfat (C), and nFF (D) between FLs and NABM (all P<0.05). ADC, apparent diffusion coefficient; nMwater, normalized water molecular signal intensity; nMfat, normalized fat signal intensity; nFF, normalized fat fraction; FLs, focal lesions; NABM, normal-appearing bone marrow.

Table 4 The correlational relationship between ADC and other parameters in two groups

ADC	nMfat		nMwater		nFF	
	r	P	r	P	r	P
NABM	−0.135	0.219	0.115	0.294	−0.145	0.186
FLs	−0.899	<0.0001	0.642	<0.0001	−0.834	<0.0001

NABM, normal-appearing bone marrow; FLs, focal lesions; ADC, apparent diffusion coefficient; nMfat, normalized fat signal intensity; nMwater, normalized water molecular signal intensity; nFF, normalized fat fraction.

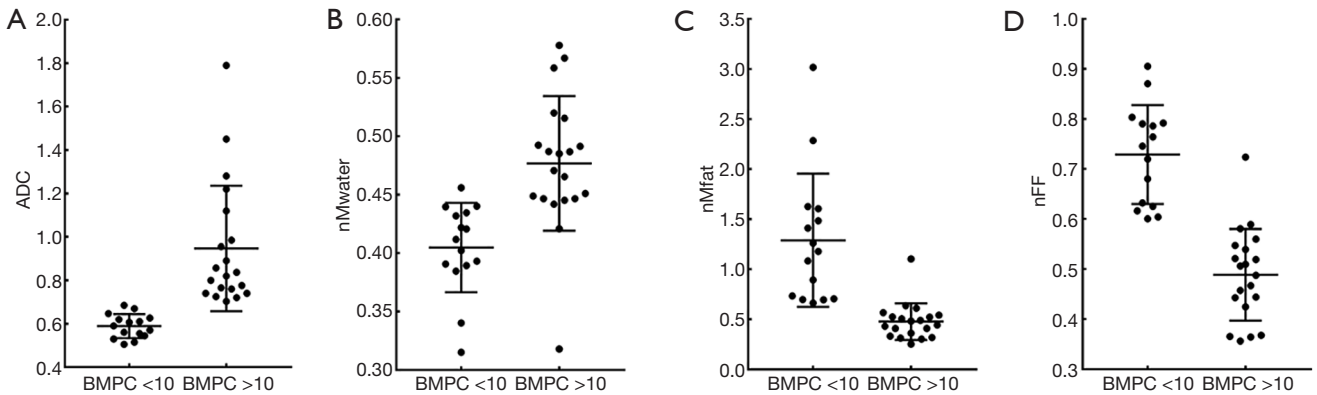

Figure 4 Scatter plot showed significant differences of ADC, nMwater, nMfat, and nFF of focal lesions between patients with BMPC <10% and BMPC >10% (A,B,C,D, all P<0.05). BMPC, bone marrow plasma cells; ADC, apparent diffusion coefficient; nMfat, normalized fat signal intensity; nMwater, normalized water molecular signal intensity; nFF, normalized fat fraction.

in *Figure 4A,B,C,D and Table 5*.

Correlation between MRI parameters and different proportions of BMPC

The proportion of BMPC highly correlated with ADC, nMwater, nMfat, and nFF values (r=0.984, 0.716, –0.938, and –0.905, P<0.05). The results are shown in *Figure 5A,B,C,D*.

Discussion

In this study, MRI indexes (ADC, nMwater, nMfat, and nFF) were measured using whole-body DWI and T1-weighted water-fat separation Dixon technique to evaluate FLs of the thoracolumbar spine in MM. The study also evaluated the possible correlation between the parameters above and the proportion of BMPC. The study yielded two important findings. First, the ADC values of FLs negatively correlated with fat signals (nMfat and nFF) in water-fat separation imaging and positively correlated with nMwater in patients with MM, which indicated that both kinds of parameters could be used to accurately evaluate the lesions in MM. According to the highest correlation with the proportion of BMPC in ADC in this study, the ADC value was still more accurate in evaluating MM lesions. Second, the ADC, nMwater, and nMfat values of the FLs in the thoracolumbar spine were different in patients with different proportions of BMPC, indicating the potential to indirectly reflect MM's severity.

Increased ADC values of bone marrow and decreased nFF in MM were observed in this study, which was consistent with the findings of a previous PET and MRI study reported by Schraml *et al.* (23). Excessive tumor cell proliferation might limit the free movement capability of extracellular water molecules in glioma than normal tissues and lead to decreased ADC values (27). Therefore, ADC in glioma could reflect the tumor's biological aggressiveness (28). However, MM is a blood cancer; thus, MM's lesions might increase the free movement capability of extracellular water molecules. Also, an increased ADC value was observed, which was proven by decreased nFF value and increased nMwater value. Therefore, it was deduced that increased ADC, decreased nFF, and increased nMwater values could indirectly indicate myeloma cell proliferation in MM.

The increased ADC value of bone marrow in patients with MM (29) might be due to the higher water content in MM lesions compared with the normal lipid-containing bone marrow, leading to a large number of water molecules in the bone marrow. Red bone marrow produced by osteolytic lesions could be reflected by the nMwater value, although some undetectable micronuclei may also have changed the nMwater values.

Table 5 Comparison of parameters between different BMPC

Parameters of MRI	BMPC <10%	BMPC >10%	P
No. of patients	15	20	–
ADC (mm^2/s)	0.59 (0.54–0.63)	0.83 (0.75–1.09)	<0.0001
nMfat	1.29±0.17	0.48±0.04	<0.0001
nMwater	0.40±0.01	0.48±0.01	<0.0001
nFF	0.23±0.03	0.09±0.01	<0.0001

BMPC, bone marrow plasma cells; ADC, apparent diffusion coefficient; nMfat, normalized fat signal intensity; nMwater, normalized water molecular signal intensity; nFF, normalized fat fraction.

The ADC values moderately correlated with nMwater values, and this relationship might partly be explained by edema around the lesion. The destruction of trabecular bone and yellow bone marrow might contribute to the effect of FLs on the bone. Baik *et al.* also reported the effect of perfusion on FLs (24).

A previous study reported a greater contrast between MM lesions and adjacent bone marrow using T2-weighted Dixon fat images (30). However, it was presumed that T1-weighted Dixon fat imaging might have higher specificity. A high correlation between ADC and nMfat and nFF was found in this study, which supported the speculation.

The nFF value was found to be <20% in this study, which was similar to a finding in a published study (24). Benign bone

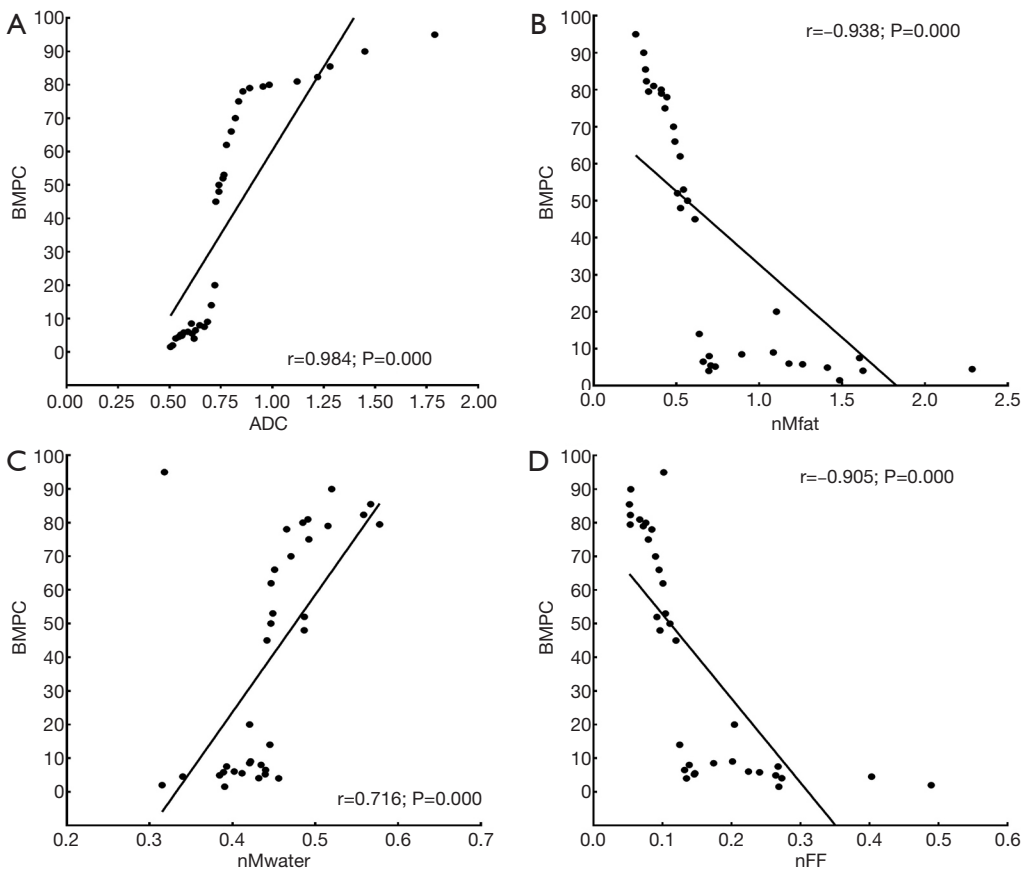

Figure 5 Scatter plot showed the BMPC was highly correlated with ADC, nMwater, nMfat, and nFF of focal lesions (r=0.984, 0.716, –0.938, –0.905, respectively, P<0.05) (A,B,C,D). BMPC, bone marrow plasma cells; ADC, apparent diffusion coefficient; nMfat, normalized fat signal intensity; nMwater, normalized water molecular signal intensity; nFF, normalized fat fraction.

marrow abnormalities contained 20–90% fat content, while most malignant bone marrow lesions contained <20% fat tissue.

The BMPC was obtained from lesions in MM by biopsy and reflected the severity of MM. They also are used for differential diagnosis between smoldering MM and MM. The indexes, such as BMPC ≥60%, free light chain ratio ≥100, and abnormal MRI (>1 lesion), were believed to be high-risk factors requiring immediate treatment. However, the use of BMPC for biopsy was unreliable due to the complex distribution of MM lesions in the skeletal system.

The FF had been reported to be a biomarker for MM to distinguish symptomatic myeloma from asymptomatic myeloma using water and fat separation MRI (31). However, no method based on MRI/PET imaging is available, which can be used to measure MM cells' quality.

The present study aimed to associate the proportion of BMPC with parameters (ADC, nMwater, nMfat, and nFF) using multi-mode MRI and found that the proportion of BMPC strongly correlated with the ADC, nMwater, nMfat, and nFF values. The data provided evidence that MRI might serve as a reliable indicator for further treatment and make up for the unreliable biopsy site.

This study had some limitations. First, the patients' follow-up information could not be collected comprehensively, and therefore it was necessary to evaluate disease progression based on conventional MRI signals before and after therapy. Second, only FLs instead of total diffused lesions were evaluated. Finally, the relationship of a diffuse degree in lesions with MM's prognosis and treatment remained unclear and required further exploration.

In conclusion, the ADC value combined with water-fat separation parameters could be used to indirectly quantitatively evaluate the extent of bone marrow infiltration of thoracolumbar spine lesions in MM. The ADC values of FLs negatively correlated with nMfat and nFF values in water-fat separation MRI and positively correlated with nMwater value in patients with MM. The MRI parameters (ADC, nMwater, nMfat, and nFF values) in MM correlated with the proportion of BMPC, helping access the proliferation of bone marrow plasmacytoma using MRI and evaluating early response therapy.

Acknowledgments

Funding: This study was supported by the National Natural Science Fund (81871342) (Shuang Xia) and the National Key Research and Development (2019YFC0120903) (Shuang Xia).

Footnote

Conflicts of Interest: All authors have completed the ICMJE uniform disclosure form (available at http://dx.doi.org/10.21037/qims-20-289). The authors have no conflicts of interest to declare.

Ethical Statement: The Ethics Committee approved the study of the First Central Hospital of Tianjin (2017N078KY), and all participants provided written informed consent before their examination.

References

1. Dimopoulos MA, Hillengass J, Usmani S, Zamagni E, Lentzsch S, Davies FE, Raje N, Sezer O, Zweegman S, Shah J, Badros A, Shimizu K, Moreau P, Chim CS, Lahuerta JJ, Hou J, Jurczyszyn A, Goldschmidt H, Sonneveld P, Palumbo A, Ludwig H, Cavo M, Barlogie B, Anderson K, Roodman GD, Rajkumar SV, Durie BG, Terpos E. Role of magnetic resonance imaging in the management of patients with multiple myeloma: a consensus statement. J Clin Oncol 2015;33:657-64.
2. Rajkumar SV, Dimopoulos MA, Palumbo A, Blade J, Merlini G, Mateos MV, Kumar S, Hillengass J, Kastritis E, Richardson P, Landgren O, Paiva B, Dispenzieri A, Weiss B, LeLeu X, Zweegman S, Lonial S, Rosinol L, Zamagni E, Jagannath S, Sezer O, Kristinsson SY, Caers J, Usmani SZ, Lahuerta JJ, Johnsen HE, Beksac M, Cavo M, Goldschmidt H, Terpos E, Kyle RA, Anderson KC, Durie BG, Miguel JF. International Myeloma Working Group updated criteria for the diagnosis of multiple myeloma. Lancet Oncol 2014;15:e538-48.
3. Hillengass J, Fechtner K, Weber MA, Bauerle T, Ayyaz S, Heiss C, Hielscher T, Moehler TM, Egerer G, Neben K, Ho AD, Kauczor HU, Delorme S, Goldschmidt H. Prognostic significance of focal lesions in whole-body magnetic resonance imaging in patients with asymptomatic

multiple myeloma. J Clin Oncol 2010;28:1606-10.
4. Kastritis E, Moulopoulos LA, Terpos E, Koutoulidis V, Dimopoulos MA. The prognostic importance of the presence of more than one focal lesion in spine MRI of patients with asymptomatic (smoldering) multiple myeloma. Leukemia 2014;28:2402-3.
5. Cavo M, Terpos E, Nanni C, Moreau P, Lentzsch S, Zweegman S, Hillengass J, Engelhardt M, Usmani SZ, Vesole DH, San-Miguel J, Kumar SK, Richardson PG, Mikhael JR, da Costa FL, Dimopoulos MA, Zingaretti C, Abildgaard N, Goldschmidt H, Orlowski RZ, Chng WJ, Einsele H, Lonial S, Barlogie B, Anderson KC, Rajkumar SV, Durie BGM, Zamagni E. Role of (18)F-FDG PET/CT in the diagnosis and management of multiple myeloma and other plasma cell disorders: a consensus statement by the International Myeloma Working Group. Lancet Oncol 2017;18:e206-17.
6. Derlin T, Weber C, Habermann CR, Herrmann J, Wisotzki C, Ayuk F, Wolschke C, Klutmann S, Kroger N. 18F-FDG PET/CT for detection and localization of residual or recurrent disease in patients with multiple myeloma after stem cell transplantation. Eur J Nucl Med Mol Imaging 2012;39:493-500.
7. Bailly C, Leforestier R, Jamet B, Carlier T, Bourgeois M, Guerard F, Touzeau C, Moreau P, Cherel M, Kraeber-Bodere F, Bodet-Milin C. PET Imaging for Initial Staging and Therapy Assessment in Multiple Myeloma Patients. Int J Mol Sci 2017;18:445.
8. Moreau P, Attal M, Caillot D, Macro M, Karlin L, Garderet L, Facon T, Benboubker L, Escoffre-Barbe M, Stoppa AM, Laribi K, Hulin C, Perrot A, Marit G, Eveillard JR, Caillon F, Bodet-Milin C, Pegourie B, Dorvaux V, Chaleteix C, Anderson K, Richardson P, Munshi NC, Avet-Loiseau H, Gaultier A, Nguyen JM, Dupas B, Frampas E, Kraeber-Bodere F. Prospective Evaluation of Magnetic Resonance Imaging and [(18)F] Fluorodeoxyglucose Positron Emission Tomography-Computed Tomography at Diagnosis and Before Maintenance Therapy in Symptomatic Patients With Multiple Myeloma Included in the IFM/DFCI 2009 Trial: Results of the IMAJEM Study. J Clin Oncol 2017;35:2911-8.
9. Derlin T, Peldschus K, Munster S, Bannas P, Herrmann J, Stubig T, Habermann CR, Adam G, Kroger N, Weber C. Comparative diagnostic performance of (1)(8)F-FDG PET/CT versus whole-body MRI for determination of remission status in multiple myeloma after stem cell transplantation. Eur Radiol 2013;23:570-8.
10. Terpos E, Moulopoulos LA, Dimopoulos MA. Advances in imaging and the management of myeloma bone disease. J Clin Oncol 2011;29:1907-15.
11. Sachpekidis C, Mosebach J, Freitag MT, Wilhelm T, Mai EK, Goldschmidt H, Haberkorn U, Schlemmer HP, Delorme S, Dimitrakopoulou-Strauss A. Application of (18)F-FDG PET and diffusion weighted imaging (DWI) in multiple myeloma: comparison of functional imaging modalities. Am J Nucl Med Mol Imaging 2015;5:479-92.
12. Malikova H. Primary central nervous system lymphoma: is whole-body CT and FDG PET/CT for initial imaging reasonable? Quant Imaging Med Surg 2019;9:1615-8.
13. Messiou C, Hillengass J, Delorme S, Lecouvet FE, Moulopoulos LA, Collins DJ, Blackledge MD, Abildgaard N, Ostergaard B, Schlemmer HP, Landgren O, Asmussen JT, Kaiser MF, Padhani A. Guidelines for Acquisition, Interpretation, and Reporting of Whole-Body MRI in Myeloma: Myeloma Response Assessment and Diagnosis System (MY-RADS). Radiology 2019;291:5-13.
14. Brioli A, Morgan GJ, Durie B, Zamagni E. The utility of newer imaging techniques as predictors of clinical outcomes in multiple myeloma. Expert Rev Hematol 2014;7:13-6.
15. Dutoit JC, Vanderkerken MA, Anthonissen J, Dochy F, Verstraete KL. The diagnostic value of SE MRI and DWI of the spine in patients with monoclonal gammopathy of undetermined significance, smouldering myeloma and multiple myeloma. Eur Radiol 2014;24:2754-65.
16. Aparisi Gómez MP, Ayuso Benavent C, Simoni P, Aparisi F, Guglielmi G, Bazzocchi A. Fat and bone: the multiperspective analysis of a close relationship. Quant Imaging Med Surg 2020;10:1614-35.
17. Andersson T, Romu T, Karlsson A, Noren B, Forsgren MF, Smedby O, Kechagias S, Almer S, Lundberg P, Borga M, Leinhard OD. Consistent intensity inhomogeneity correction in water-fat MRI. J Magn Reson Imaging 2015;42:468-76.
18. Shen W, Gong X, Weiss J, Jin Y. Comparison among T1-weighted magnetic resonance imaging, modified dixon method, and magnetic resonance spectroscopy in measuring bone marrow fat. J Obes 2013;2013:298675.
19. Garau LM, Guerrieri D, De Cristofaro F, Bruscolini A, Panzironi G. Extraocular muscle sampled volume in Graves' orbitopathy using 3-T fast spin-echo MRI with iterative decomposition of water and fat sequences. Acta Radiol Open 2018;7:2058460118780892.
20. Sollmann N, Dieckmeyer M, Schlaeger S, Rohrmeier A, Syvaeri J, Diefenbach MN, Weidlich D, Ruschke S,

Klupp E, Franz D, Rummeny EJ, Zimmer C, Kirschke JS, Karampinos DC, Baum T. Associations Between Lumbar Vertebral Bone Marrow and Paraspinal Muscle Fat Compositions-An Investigation by Chemical Shift Encoding-Based Water-Fat MRI. Front Endocrinol (Lausanne) 2018;9:563.
21. Baum T, Yap SP, Dieckmeyer M, Ruschke S, Eggers H, Kooijman H, Rummeny EJ, Bauer JS, Karampinos DC. Assessment of whole spine vertebral bone marrow fat using chemical shift-encoding based water-fat MRI. J Magn Reson Imaging 2015;42:1018-23.
22. Ueda Y, Miyati T, Ohno N, Motono Y, Hara M, Shibamoto Y, Kasai H, Kawamitsu H, Matsubara K. Apparent diffusion coefficient and fractional anisotropy in the vertebral bone marrow. J Magn Reson Imaging 2010;31:632-5.
23. Schraml C, Schmid M, Gatidis S, Schmidt H, la Fougere C, Nikolaou K, Schwenzer NF. Multiparametric analysis of bone marrow in cancer patients using simultaneous PET/MR imaging: Correlation of fat fraction, diffusivity, metabolic activity, and anthropometric data. J Magn Reson Imaging 2015;42:1048-56.
24. Baik JS, Jung JY, Jee WH, Chun CW, Kim SK, Shin SH, Chung YG, Jung CK, Kannengiesser S, Sohn Y. Differentiation of focal indeterminate marrow abnormalities with multiparametric MRI. J Magn Reson Imaging 2017;46:49-60.
25. Messiou C, Giles S, Collins DJ, West S, Davies FE, Morgan GJ, Desouza NM. Assessing response of myeloma bone disease with diffusion-weighted MRI. Br J Radiol 2012;85:e1198-203.
26. Latifoltojar A, Hall-Craggs M, Rabin N, Popat R, Bainbridge A, Dikaios N, Sokolska M, Rismani A, D'Sa S, Punwani S, Yong K. Whole body magnetic resonance imaging in newly diagnosed multiple myeloma: early changes in lesional signal fat fraction predict disease response. Br J Haematol 2017;176:222-33.
27. Lecouvet FE. Whole-Body MR Imaging: Musculoskeletal Applications. Radiology 2016;279:345-65.
28. Ahlawat S, Khandheria P, Subhawong TK, Fayad LM. Differentiation of benign and malignant skeletal lesions with quantitative diffusion weighted MRI at 3T. Eur J Radiol 2015;84:1091-7.
29. Padhani AR, van Ree K, Collins DJ, D'Sa S, Makris A. Assessing the relation between bone marrow signal intensity and apparent diffusion coefficient in diffusion-weighted MRI. AJR Am J Roentgenol 2013;200:163-70.
30. Danner A, Brumpt E, Alilet M, Tio G, Omoumi P, Aubry S. Improved contrast for myeloma focal lesions with T2-weighted Dixon images compared to T1-weighted images. Diagn Interv Imaging 2019;100:513-9.
31. Kapoor P, Rajkumar SV. Smoldering Multiple Myeloma: To Treat or Not to Treat. Cancer J 2019;25:65-71.

Cite this article as: Ji X, Huang W, Dong H, Shen Z, Zheng M, Zou D, Shen W, Xia S. Evaluation of bone marrow infiltration in multiple myeloma using whole-body diffusion-weighted imaging and T1-weighted water-fat separation Dixon. Quant Imaging Med Surg 2021;11(2):641-651. doi: 10.21037/qims-20-289

Supplementary material

Supplementary material 1. Normalization

Firstly, we had explored the signal consistency of the fat in the same phase direction with lesions in all patients with multiple myeloma (MM) (*Figure S1*). Two radiologists (S Xia, X Ji with 22 and 10 years of experience) drew the signal of each lesion, normal bone marrow, and subcutaneous fat at the same level in T1-weighted water-fat separation Dixon.

Secondly, we verified the normal distribution of subcutaneous fat signal, drew the histogram, then tested the consistency between the two radiologists.

Third, the signal intensity on both water and fat phase drawn by two radiologists showed normal distribution (*Figure S2*).

Fourth, the subcutaneous fat signals measured by the two observers were highly consistent, R^2=0.936, 0.926 (*Figure S3*).

Thus, we used the subcutaneous fat signal as a reference to the lesions.

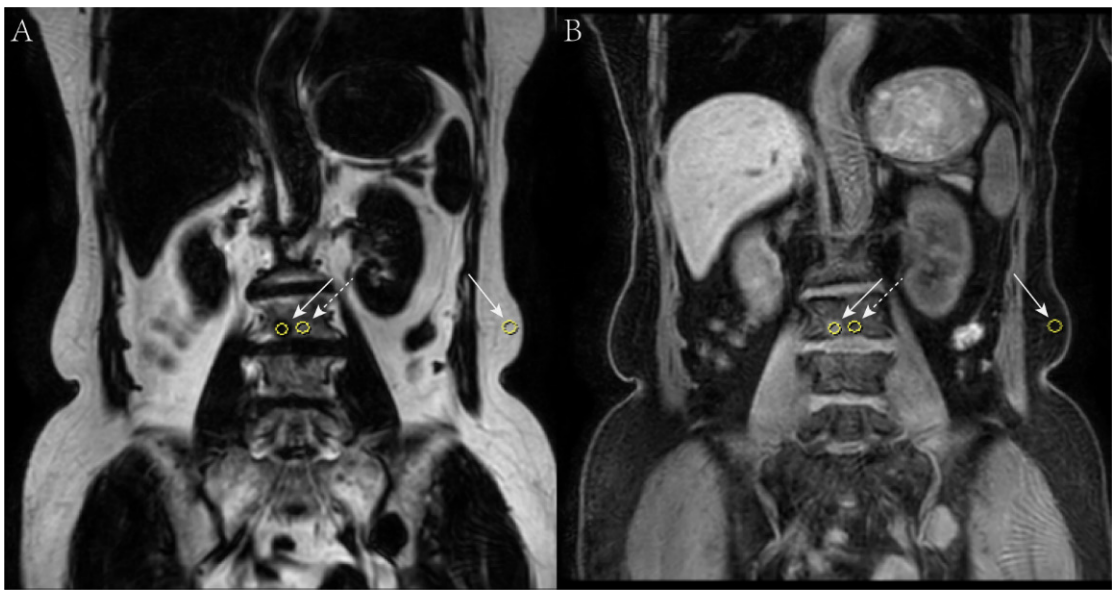

Figure S1 The coronal fat phase image of the thoracolumbar spine shows the focal lesion (the solid arrow), NABM of the same vertebral body (the virtual arrow), subcutaneous fat of the same vertebral body (another solid arrow) (A); the coronal water phase image of the thoracolumbar spine shows the focal lesion (the solid arrow), NABM of the same vertebral body (the virtual arrow), subcutaneous fat of the same vertebral body (another solid arrow) (B). NABM, normal-appearing bone marrow.

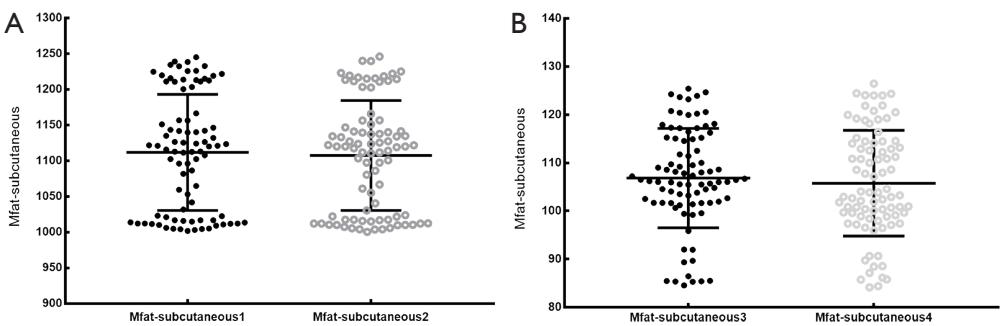

Figure S2 The signal intensity on both water and fat phase drawn by 2 radiologists showed normal distribution. Mfat, fat signal intensity.

http://dx.doi.org/10.21037/qims-20-289

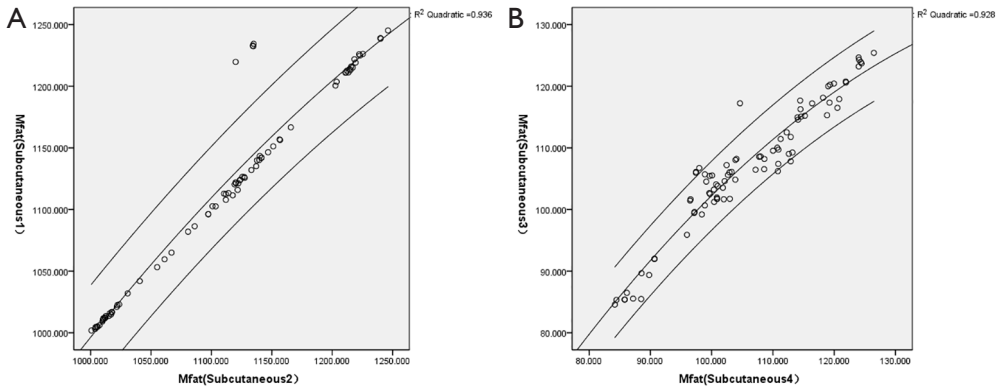

Figure S3 Verification of the inter-group consistency of subcutaneous fat signals sketched by two radiologists. The subcutaneous fat signals measured by the two observers were highly consistent, R^2=0.936, 0.926. Mfat, fat signal intensity.

Supplementary material 2. The selection of FLs on high quality images (Figure S4)

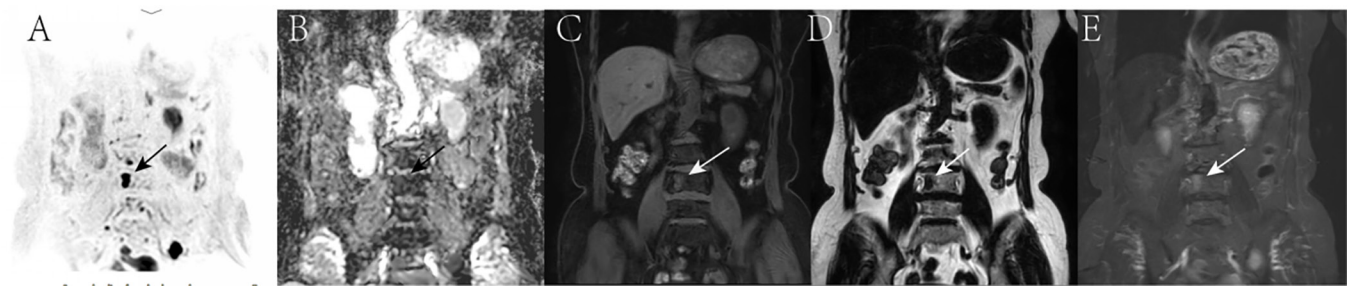

Figure S4 A focal lesion was clearly shown on all sequences. The focal lesion shows hyperintensity on coronal DWI image (A), isointensity on ADC image (B), T2-STIR image (C), hypointensity on fat phase image (D), and water phase image (E). DWI, diffusion-weighted imaging; STIR, short-time inversion recovery; ADC, apparent diffusion coefficient.

Supplementary material 3. The inclusion and exclusion criteria for patients (Figure S5)

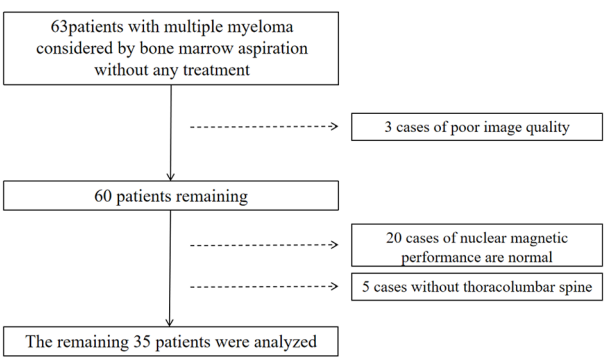

Figure S5 Flowchart of enrolled patients.

http://dx.doi.org/10.21037/qims-20-289

Supplementary material 4. High quality of images

(I) We adopted a standardized scanning scheme and a respiratory gating scheme to ensure a high SNR. (II) We used a high b value (800 s/mm^2) to reduce signal the background tissue. (III) We chose images without motion artifacts and image deformation for analysis. *Figure S6* below shows the high quality of the images (reference: Messiou C, Hillengass J, Delorme S, *et al.* Guidelines for Acquisition, Interpretation, and Reporting of Whole-Body MRI in Myeloma: Myeloma Response Assessment and Diagnosis System (MY-RADS). Radiology 2019;291:5-13).

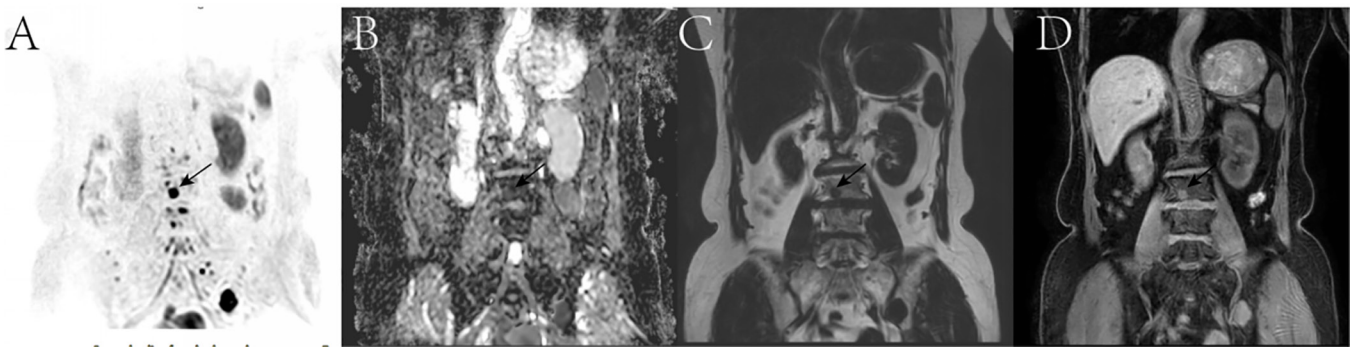

Figure S6 (A,B,C,D) The DWI, ADC, fat phase, and water phase images are displayed respectively. No artifacts were seen and the lesions were clearly shown (arrows). DWI, diffusion-weighted imaging; ADC, apparent diffusion coefficient.

Supplementary material 5. Correlation between MRI parameters of focal lesions and different BMPC (Figure S7)

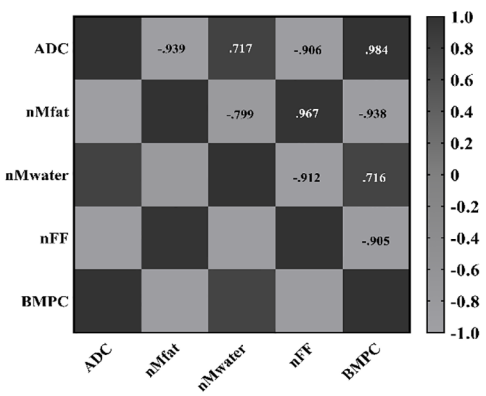

Figure S7 Correlation matrix showed correlation between MRI parameters of FLs and different BMPC. Strong correlation between ADC, nMfat, nMwater, nFF of focal lesions and BMPC was found (P<0.05). BMPC, bone marrow plasma cells; FLs, focal lesions; ADC, apparent diffusion coefficient; nMfat, normalized fat signal intensity; nMwater, normalized water molecular signal intensity; nFF, normalized fat fraction.

http://dx.doi.org/10.21037/qims-20-289

Supplementary material 6 (Table S1)

Table S1 The clinical and biological data of the enrolled patients

Patient	Gender	Age (years)	BMPC (%)	Cr (μmol/L)	HGB (g/L)	Ca (mmol/L)	Treatments received
1	1	60	1.5	44.4	110	2.2	TAD
2	0	50	2	71	129	2.37	RD
3	0	69	4	110.5	138	3.08	BCD
4	0	58	4.06	53	93	2.19	BCD
5	1	66	4.5	87.4	121	2.14	BD
6	1	62	4.9	82.7	100	223	MPR
7	1	61	5.2	73	112	1.82	PAD
8	1	36	5.5	77.5	134	2.52	BCD
9	1	65	5.8	64	98	2.13	BCD
10	0	44	6	52.9	134	2.76	BCD
11	0	38	6.5	49.5	137	1.92	BCD
12	1	57	7.5	52.9	134	2.38	MPR
13	1	63	8	66	94	2.35	BCD
14	1	44	8.5	91	100	2.55	BCD
15	0	44	9	66.6	140	2.33	RCD
16	1	44	14	60.7	102	2.33	RCD
17	1	48	20	82.8	95	2.58	BCD
18	1	52	45	94.6	99	2.52	BCD
19	1	67	48	106	101	2.47	BD
20	0	52	50	102.9	124	2.48	BCD
21	1	52	52	72.8	141	2.32	RCD
22	0	45	53	56.1	95	2.21	BD
23	1	54	62	80.1	98	2.41	VTD
24	0	53	66	80.5	96	2.35	RCD
25	0	39	70	119.1	93	3.45	PAD
26	1	63	75	72.8	94	1.86	BCD
27	0	66	78	194.5	95	2.23	BCD
28	0	32	79	56	113	2.21	BD
29	1	58	79.5	237.1	94	1.76	BCD
30	1	36	80	70.5	112	2.18	BCD
31	0	62	81	323.3	98	2.51	TCD
32	0	55	82.3	40.3	93	1.95	BCD
33	0	41	85.5	46.7	136	2.38	TAD
34	1	47	90	22.2	90	2.39	TAD
35	1	52	95	51.6	90	1.75	TCD

Gender, female-0, male-1; BMPC, bone marrow plasma cells; Cr, creatinine; HGB, hemoglobin; Ca, calcium; BCD, bortezomib, cyclophosphamide, dexamethasone); BD, bortezomib, dexamethasone; MPR, melphalan, prednisone, lenalidomide; PAD, bortezomib, adriamycin, dexamethasone; RCD, lenalidomide, cyclophosphamide, dexamethasone; RD, lenalidomide, dexamethasone; TAD, thalidomide, adriamycin, dexamethasone; TCD, thalidomide, cyclophosphamide, dexamethasone; VTD, bortezomib, thalidomide, dexamethasone.

http://dx.doi.org/10.21037/qims-20-289